Article

# Ultrasensitive Detection of MicroRNAs with Morpholino-Functionalized Nanochannel Biosensor

Tangbin Liao, Xiaorui Li, Qian Tong, Kai Zou, Hang Zhang, Lina Tang, Zhongyue Sun, and Guo-Jun Zhang

*Anal. Chem.*, **Just Accepted Manuscript** • Publication Date (Web): 21 Apr 2017

# Ultrasensitive Detection of MicroRNAs with Morpholino-Functionalized Nanochannel Biosensor

Tangbin Liao, [+] Xiaorui Li, [+] Qian Tong, Kai Zou, Hang Zhang, Lina Tang, Zhongyue Sun,* Guo-Jun Zhang*

[a]School of Laboratory Medicine, Hubei University of Chinese Medicine, 1 Huangjia Lake West Road, Wuhan 430065, China

[+]These authors contributed equally to this work.

*Corresponding author: Tel: +86-27-68890259, Fax: +86-27-68890259

E-mail: zhanggj@hbtcm.edu.cn, shui10123@aliyun.com

**Abstract**

Here we demonstrate a phosphorodiamidate morpholino oligos (PMO)-functionlized nanochannel biosensor for label-free detection of microRNAs (miRNAs) with ultrasensitivity and high sequence-specificity. PMO, as a capture probe, was covalently anchored on the nanochannel surface. Because of the neutral character and high sequence-specific affinity of PMO, hybridization efficiency between PMO and miRNAs was enhanced, thus decreasing background signals largely and improving the detection specificity and sensitivity highly. The miRNAs detection was realized through observing the change of surface charge density when PMO/miRNAs hybridization occurred. Not only could the developed biosensor specifically discriminate complementary miRNAs (Let-7b) from non-complementary miRNAs (miR-21) and one-base mismatched miRNAs (Let-7c), but also it could detect target miRNAs in serum samples. In addition, this nanochannel based biosensor attained a reliable limit of detection down to 1 fM in PBS and 10 fM in serum sample, respectively. It is expected that such a new method will benefit miRNA detection in clinical diagnosis.

**Keywords:** Nanochannels; Biosensor; Label-Free Detection; miRNAs; Hybridization

## INTRODUCTION

MicroRNAs (miRNAs) are a class of single-strand, regulation of gene expression, small and short noncoding RNAs with 18-24 nucleotides long. Recently, amount of studies have indicated that miRNAs play important roles in a wide range of physiological processes, and various biological processes.[1,2] Specifically, their aberrant expressions are closely associated with various human diseases, such as cancers, diabetes, and neurodegenerative disease.[3,4] miRNAs can thus be employed as new biomarkers for early diagnosis and treatment of major diseases like cancers.[5-7] Currently, lung cancer is one of the most common cancers in the world because of its high incidence. The prognosis of lung cancer is usually challenging because effective methods for early diagnosis and treatment are lacking. Recently, let-7 family members have become increasingly important in lung cancer because the amount of let-7 in lung cancer significantly decreases compared with that in normal lung tissue. Thus let-7 members could be used as diagnostic biomarkers for breast cancer screening and disease progression.[8, 9] At present, conventional technical platforms for miRNAs profiling include northern blotting,[10,11] molecular cloning,[12] microarrays,[13,14] real-time quantitative polymerase chain reaction (qRT-PCR),[15,16] etc. Nevertheless, those approaches have some disadvantages including high detection limit, requirement of a large amount of sample, and tedious preparation procedures. Therefore, it is still a challenging job to develop a sensitive and specific biosensor for let-7 detection.

To date, nanochannel-based biosensors have been developed considerably because they are highly specific and sensitive, and they have been proven to be a

novel biosensing platform.[18-30] In these nanochannels, conical nanochannel-based biosensors have shown outstanding performance, including not only the relative ion current change ratios (ratios defined by $(I–I_0)/I_0$, where $I_0$ is the initial current), but also ion selective permeability dependent sensibly on density of surface charge, especially at the tip opening of the channel.[31-33] For example, Li et al.[19] reported the zinc ions and $HPO_4^{2-}$ anions sensor based on 2, 2'-dipicolylamine (DPA)-modified multi-nanochannels. This sensor showed specific detection of zinc ions and this zinc-ion-chelated on the nanochannels surface could secondarily detect $HPO_4^{2-}$ anions. Sun et al.[18] developed a reaction-based biomimetic nanochannel sensor for detection of Cys with high selectivity and sensitivity in real sample. Wen et al.[23] used layer-by-layer assembly method to immobilize p-sulfonatocalix[4]-arene (SCX4) on nanochannel surface. This sensing system has been used for acetylcholine (Ach) detection with high sensitivity and selectivity. Siwy's group[25] introduced a monoclonal antibody (mAb F26G3) modified nanochannel for γ-D-glutamic acid (γDPGA) detection from Bacillus anthracis. Sun et al.[30] and Ali et al.[28], respectively, reported a simple, highly selective and label-free sensing system, in which deoxyribonucleic acid (DNA) or peptide nucleic acid (PNA)-modified nanochannel was proposed for the sequence-specific DNA detection. In these work, DNA or PNA, has been employed as probe molecule and immobilized on the channel surface through various modification methods. Because of electrostatic hindrance between DNA/DNA duplex, it is not preferable to use DNA as a capture probe for highly sensitive detection in nanochannel biosensor. The PNA-modified nanochannel was

reported to have a notable sensitivity.[28] Nevertheless, PNA has limitations on length synthesis (22 bp in maximum), which is not suitable for real applications. For example, a longer probe length is usually required in the process of gene expression. So it is still interesting to develop a simple, cost-effective and label-free nanochannel biosensor for miRNAs detection by choosing a unique probe molecule.

Phosphorodiamidate Morpholino Oligos (PMO), belonging to the 3rd generation of antisense oligonucleotides, was discovered in 1985 by summerton.[34, 35] PMO is a synthetic DNA analog with a neutral backbone of morpholine rings. Compared with PNA, PMO shows not only higher solubility in aqueous solutions, but also more flexible in length. For example, Zhang et al.[36] reported a morpholino modified silicon nanowires field-effect transistor (FET) biosensor for label-free and sequence-specific detection of DNA. This unique sensing platform exhibited good specificity and sensitivity. Recently, a label-free DNA electrochemical biosensor, in which morpholino functioned as capture probe was reported.[37] Furthermore, a colorimetric method was also proposed for label-free DNA detection by using a new type of morpholino/Au nanoparticle conjugates. When morpholino-DNA hybridization took place, nanoparticle assemblies could be formed, leading to the colorimetric target recognition.[38] In a word, PMO has a good stability, solubility and specificity, making it an ideal probe molecule for nanochannel sensing. Recently, electrochemical detection systems have been developed for DNA and single nucleotide polymorphisms (SNPs) sensing by measuring the flux of electroactive probe ions flowing through a PMO modified porous anodic alumina (PAA) nanochannel

array.[39-41] A thin layer of Au film acting as an electrochemical detector was sputtered on one side of PAA nanochannel, and negatively charged $Fe(CN)_6^{3-}$ was used as the electroactive probe to give an electrochemical signal. This electrochemical method is unable to monitor the surface charge change of non-conductive PAA nanochannel directly because it requires additional electrochemical indicator. Moreover, the sensitivity of these methods is not satisfactory yet.

Alternatively, detection approach of measuring the ionic current flowing through nanochannels can directly demonstrate the charge on the channel surface, making the detection direct, sensitive and simple. In this paper, we report a unique nanochannel-based biosensor for miRNA detection by monitoring ionic current caused by surface charge change during PMO immobilization and PMO/miRNA hybridization. In this system, PMO as a probe is modified on the channel surface by covalent bond, and miRNA detection is realized via PMO/miRNA hybridization. While the hybridization event takes place, the membrane current change can be recorded, resulting in the surface charge density change of the nanochannel. Last but not least, the complementary, one-base mismatched and noncomplementary miRNA sequences are employed to demonstrate the high sequence specificity of this sensing platform. Most importantly, this sensor could be applied for miRNAs detection in real serum samples.

## EXPERIMENTAL SECTION

### Materials and miRNA Sequences

Poly (ethylene terephthalate) (PET, 12-μm thick) membranes were irradiated with Ar ion beam of energy 18 MeV/nucleon (Tsinghua University, Beijing, China). The track density is about $4\times10^5/cm^2$. The length of PMO and miRNA sequences is 22 base pairs, respectively. The sequence of the PMO probe is 5′-$H_2N$-AACCACACAACCTACTACCTCA-3′. The sequences of miRNAs are 5′-UGAGGUAGUAGGUUGUGUGGUU-3′ (complementary, let-7b), 5′-UGAGGUAGUAGGUUGUAUGGUU-3′ (one-base mismatched, let-7c), 5′-UAGCUUAUCAGACUGAUGUUGA-3′ (non- complementary, miR-21). Sodium hydroxide (NaOH) and formic acid (HCOOH) were purchased from Sinopharm Chemical Reagent Shanghai Co. Ltd. (Shanghai, China). Bovine serum albumin (BSA), RNaseZap, 1-ethyl-3-(3- dimethyllaminopropyl) carbodiimide (EDC, 98%) and N-hydroxysulfosuccinimide (sulfo-NHS, 98.5%) were purchased from Sigma-Aldrich (St. Louis, MO, USA). All solutions were prepared in ultrapure water at molecular biology level, which was purchased from Genom Biological Pharmaceutical Technology co., LTD (Hangzhou, China).

**Fabrication of conical nanochannels**

The chemical etching of 12 μm-thick PET membrane was conducted according to our previous work.[30] Conical nanochannels were obtained by the following two steps: In the first step, UV light (365 nm) was irradiated on each side of the PET membranes for 4 h. The second step was the asymmetric etching process. One side of the cell was filled with etching solution and the other side was added with stopping solution to neutralize the etching solution, further slowing down the etching process.

After chemical etching, the film was washed and immersed in distilled water to remove residual salts. Field emission-scanning electron microscopy (FE-SEM, Zeiss SIGMA, Germany) was used to characterize the nanochannel size of both sides. As seen in Figure S1, the diameter of large opening of conical nanochannel was found to be about 1.1 μm and the small opening was approximately 51 nm.

**PMO Immobilization**

After etching, the nanochannel surface carrying the carboxylic groups (-COOH) was obtained. The membrane was immersed in a 15 mg/ml EDC and 3 mg/ml sulfo-NHS mixture solution for 40 min. And the film was washed thoroughly with pure water. Then PMO (10 μM, pH 7.1) solution was added onto two sides of the unmodified PET film for 12 h. Subsequently, the film was washed with distilled water to remove unreacted probe PMO and incubated with 10 mg/mL BSA solution for 1 h to block the un-reacted binding sites, followed by being washed by distilled water. The current-voltage (I-V) curves measurement by employing 0.5×PBS (pH 7.1) as electrolyte was conducted to prove the success of the modification.

**PMO-miRNA hybridization**

The PMO-modified nanochannel membrane was exposed to miR-21 solutions and incubated at 37°C for 4 h. After PMO-miRNA was hybridized, the film was cleaned with 0.5×PBS (pH 7.1) solution and distilled water, respectively, to remove the unhybridized miR-21. After washing, the ion flux was measured using 0.5×PBS (pH 7.1) as an electrolyte. The same procedure was repeated when let-7c and let-7b were hybridized with probe PMO on the channel surface, respectively.

### Ion currents measurement

A Keithley 6487 picoammeter (Keithley Instruments, Cleveland, OH, USA) was used for the measurement of in currents. Ag/AgCl electrodes were applied for the transmembrane potential across nanochannel. Electrolyte solution, 0.5×PBS (pH 7.1), was filled in each half of cells after PET film was fixed. Then the data recording was conducted with a scanning voltage varying from -2 V to +2 V for 40 s in 0.5×PBS (pH 7.1). Each measurement was repeated 5 times to get the average current value at different voltages.

### Characterizations

The nanochannel diameter was determined by FE-SEM. X-ray photoelectron spectroscopy (XPS) spectra of the nanochannels were obtained by an ESCALAB 250Xi XPS (Thermo Fisher, America) and the source gun types were Al and Ka. Laser scanning confocal microscopy (LSCM) image of the inner membrane surface was obtained by a confocal laser scanning microscope (Zeiss LSM710, Germany).

## RESULTS AND DISCUSSION

### Mechanism

The working mechanism of the PMO-functionalized nanochannel biosensor for the label-free detection of miRNA is depicted in Figure 1. At first, through chemical etching method, the conical nanochannels are prepared in PET film. After the nanochannel is prepared, ionized carboxylic groups ($-COO^-$) are exposed on the

unmodified conical-shaped nanochannels surface, leading to a negatively charged surface. Secondly, the amine-modified PMO is covalently coupled with the carboxylic groups by using a mixture of EDC and sulfo-NHS,[42] through which PMO is immobilized on the channel surface. Subsequently, negatively charged BSA is used for blocking the unbound sites, leading to more negative charges on the surface. When target miRNA is hybridized with probe PMO, charge density of the nanochannel surface dramatically changes due to the contribution of negative charges of phosphate backbone of miRNA nucleotide. The hybridization between probe and target is monitored by recording the I-V curves.

**Surface Modification of Nanochannels**

In this experiment, the surface modification process was conducted by measuring the transmembrane ionic current with 0.5×PBS (pH 7.1) solution filled in two halves of cells. Before and after surface modification, I-V curves of conical nanochannel were recorded in Figure 2A. As discussed, the unmodified conical-shaped PET nanochannel surface was negatively charged, and I-V curve of the bare nanochannel acted as the control. After the channel surface was covalently coupled with PMO probe, a decrease in the negative charge of the nanochannel was obtained. Upon introduction of uncharged PMO, the charge on the inner channel surface significantly decreased, which leads to remarkable ion current decrease. The curve was observed to be almost a straight line. As shown, before modification, permselective transport of ions through the nanochannel was measured at a potential of -2 V, and an average rectified ion current of -0.535 mA was obtained. Immobilization of PMO led to a

54 % decrease in rectified ion current at -2 V. That is because neutral PMO probe diminishes the negative charge on the nanochannel surface. The change in the I-V characteristics before and after modification indicates that PMO was successfully attached onto the nanochannel surface. Afterwards, BSA was employed to block the unmodified sites on the surface. As the negatively charged BSA molecule increased the negative channel surface charge once again, the rectified ionic current measured at -2 V was raised from -0.264 mA to - 0.359 mA.

To further verify the success of the modified process, XPS was used to detect the content of phosphorus and nitrogen elements contained in PMO. In Figures 2B and 2C, the XPS characterizations were conducted on the unmodified nanochannel membrane as the control (black line), and the PMO-modified membrane (green line), respectively. On the unmodified PET film surface, only C 1s and O 1s peaks were clearly observed. After PMO was introduced to the channel surface (green line), it was clearly seen that, both N 1s (399 eV) peak (Figure 2B) and P 2p (133 eV) peak (Figure 2C) appeared, further indicating that probe PMO was immobilized on the nanochannel surface. All the above data verify the success of the PMO modification process on the nanochannel surface.

**Stability**

The stability of PMO functionalized PET film in 0.5×PBS (pH 7.1) was also investigated by measuring voltage and current as a function of time. As shown in Figure S2, red trace represents the voltage, and blue one represents the corresponding transmembrane current. With the voltage ranging from -2 V to +2 V for 520 s (red

trace), negligible change on the amplitude and shape of current curves (blue trace) appeared. The data show that the stability of the modified nanochannel has not been affected when the nanochannel is polarized under different potentials in the electrolyte solution. The result indicates that it could be used for miRNA detection.

**Optimization of hybridization time**

In this system, the hybridization temperature was fixed at 37 °C by considering the normal body temperature. The hybridization time was investigated when let-7b was applied to the PMO-modified nanochannel sensor. As shown in Figure S3, when 1 nM let-7b was interacted with the PMO-modified nanochannel sensor, the relative ion current change ratios: $(I - I_0)/I_0$ increased with the hybridization time from 30 to 180 min. In the period of 30-120 min, the ratios increased sharply along with the increasing time. The hybridization tended to be stable after 120 min. In the experiment, the optimal hybridization time was chosen as 120 min.

**Specificity**

The specificity of the PMO-functionalized nanochannel biosensor was performed by applying complementary target miRNA, non-complementray target miRNA, and mismatched target to the sensor, as illustrated in Figure 3A. The functionalized nanochannel membrane was immersed in 1 nM miR-21, let-7c, and let-7b at 37 °C for 2 h, respectively. Then, the film was washed with 0.5×PBS (pH 7.1) to remove physically adsorbed miRNA molecules. The hybridization on the channel surface was monitored by transmembrane current. Figure 3B shows the ion current of the probe PMO-modified nanochannel incubated with 0.5×PBS, 1 nM miR-21, let-7c, and

let-7b, respectively. 0.5×PBS was acted as the control (black line) in this experiment. Upon exposure of the modified channels to miR-21 solution, only slight change in the relative ion current change ratios was observed. Addition of let-7c resulted in a negligible response, probably owing to some nonspecific adsorption. When the film was interacted with let-7b, the current increased remarkably. Figure 3C presents current change ratios of the modified nanochannel while 1 nM concentration of the above-mentioned 3 miRNA strands was applied. For let-7c, the relative ion current change ratio was larger than that of miR-21, but still much smaller than that of let-7b. It is obvious that the relative ion current change ratio for let-7b was much larger than that of let-7c and miR21. The data indicate that the PMO-functionalized nanochannel biosensor can distinguish let-7b from let-7c and miR21, exhibiting a remarkable specificity.

**Verification of PMO-miRNA hybridization by fluorescent imaging and XPS**

The hybridization event occurring on the nanochannels surface was verified by LSCM. As shown in Figure 4A, two Cy3-labeled target miRNA (Cy3-let-7b and Cy3-miRNA-21), respectively, were used to hybridize with the immobilized probe PMO. When the probe modified nanochannels were immersed to 1 nM Cy3-miRNA-21 solutions at 37 °C for 2 h, negligible fluorescent signal was seen. The result reveals that the hybridization of PMO with miRNA-21 did not occur. However, the strong fluorescent signal appeared after hybridization between PMO and Cy3-let-7b occurred, indicating that Cy3-let-7b has successfully been hybridized with the probe PMO on the nanochannel surface. In addition, the fluorescent signal showed

that the membrane thickness was ca. 12 ± 0.5 μm, which is consistent with its actual thickness. The data prove that let-7b has been hybridized with probe PMO on the nanochannel surface as anticipated.

To further verify the successful hybridization between PMO and miRNA, XPS was used to detect the content of sulphur elements contained in Cy3 when cy3-let-7b was hybridized with probe PMO, as above-mentioned. As shown in Figures 4B, 4C and 4D. The XPS characterizations were conducted on the PMO-modified membrane (green), and cy3-let-7b hybridization membrane (yellow line), respectively. On the PMO-modified PET film surface, only C 1s and O 1s, N1s (Figures 4B), P2p (Figures 4C) peaks were clearly observed. After Cy3-let-7b was hybridized with probe PMO on the nanochannel surface, it was clearly seen that a S2p (166 eV) peak appeared (Figures 4D), further indicating that Cy3-let-7b has been hybridized with probe PMO. All the above data verify the successful hybridization of PMO and let-7b on the surface of the PET nanochannel.

**Sensitivity**

For purpose of investigating the sensitivity of the nanochannel-based biosensor, various concentrations of let-7b (from 100 aM to 1 nM) were introduced to hybridize with the PMO-modified nanochannel. And the responses of the nanochannel biosensor to different concentrations of let-7b were shown in Figure 5A. It is clear that the relative ion current change increased generally with the increased concentration from 100 aM to 1 nM. This sensor displayed a good response to let-7b in a concentration range. A blank control experiment with 0.5×PBS without any

miRNA was conducted to show the noise value and dashed line indicates the value of three-fold noise in Figure 5B. Based on the fact that the signal exceeds the background by 3 times, the sensitivity of the nanochannel sensor was found to be 1 fM, which is 1 order magnitude higher than that of the previous work regarding PNA-miRNA hybridization. [43]

Cheng et al. reported a Au nanoparticles (NPs) quenching-based competition assay system for label-free miRNA detection. This method was sensitive and specific to target miRNA with detection limit down to 3.8 pM.[44] Trau et al. introduced elevated affinity interaction to design an amplification-free miRNA detection assay with detection limit down to 10 fM.[45] Cai et al. reported a double-strand displacement based fluorescence sensor for quencher-free miRNA detection, in which the detection limit is 5 nM.[46] Miao et al. described a hybridization chain reaction based silver nanoparticles colorimetric method for miRNA detection and the detect limit is 1 pM.[47] Luo et al. developed an DNA probe modified reduced graphene oxide coated surface plasmon resonance (SPR) biosensor for real-time monitoring of miRNA-DNA hybridization. Duplex-specific nuclease (DSN) was introduced to amplify signal and the sensitivity of this sensor is as high as 3 fM.[48] Our group has recently developed a gold nanoparticles (AuNPs)-functionalized graphene FET biosensor for miRNA detection with ultra sensitivity and high specificity.[43] This system applied AuNPs to amplify detection signal and introduced capture probe PNA to improve the specificity and sensitivity. The detection limit is 10 fM.

The various methods for miRNA sensing based on probe-miRNA hybridization

were illustrated in Table S1. Compared with other label-free miRNA detection methods, the nanochannel-based miRNA sensor has special 3D nanoscale environment. Moreover, morpholino, as a probe molecule, does not contain charges, which eliminates the background signal. Not only is the sensor unnecessary to introduce signal amplification strategy, but also it could reach a reliable detection limit of 1 fM for target miRNA. The sensitivity of the developed method is about 1 order of magnitude higher than that reported by FET, 3 orders of magnitude higher than that reported by photoluminescence, and colorimetric method, and 1 order of magnitude higher than that reported by electrochemistry, respectively。

**Reproducibility and Reusability**

To evaluate the reproducibility of the nanochannel sensor, the relative ion current change ratios (at -2 V) of 4 functionalized nanochannels in the presence of 1 nM concentration of Let-7b were obtained (Figure 6A). As seen, the relative ion current change ratios did not change remarkably from 4 parallel experiments, indicating that multiple nanochannels give rise to similar results on the detection of miRNA.

Reusability of the PMO modified nanochannels biosensors was also investigated (Figure 6B). 4 successive experiments were repeated at the same nanochannel by immersing the biosensors into absolute ethyl alcohol solution at room temperature for 4 h on shaking table for denaturation, and subsequently applying the same concentration of Let-7b to the nanochannel for re-hybridization. By repeating the process, denaturation and re-hybridization were successively performed. When denaturation was carried out, the current decreased. When the hybridization was

conducted, the current increased again. Reversible variation of the ionic current of nanochannels at -2 V (re-hybridization: red squares and denaturation: blue squares) shows that this biosensor has a reliable reusability and can be re-used for multiple times.

**Serum sample analysis**

In order to further investigate the practical application of the nanochannel-based biosensor, we challenged miRNA detection in real samples. Bovine serum was used as real sample, and target miRNA was spiked into the serum with varying concentrations. In 5 % fetal bovine serum sample containing various concentrations of let-7b (from 100 aM to 1 nM), the sensor still maintained high detection ability to target miRNA. As shown in Figure 7A, it was found that the relative ion current change increased generally with the increased concentrations of let-7b from 100 aM to 1 nM in 5 % fetal bovine serum sample. In a range of let-7b concentration, this nanochannel sensor showed good response to let-7b. Similar to the above-mentioned discussion, a blank control test with 5 % fetal bovine serum without any miRNA was performed. Dashed line in Figure 7B indicates the value of three-fold noise. The detection limit of the sensor was determined to be 10 fM. The results demonstrate that the biosensor still works well in serum samples, showing its potential of being applied in the practical applications.

## CONCLUSIONS

In summary, we have developed a very simple and facile strategy to fabricate a

novel PMO-modified nanochannel sensing platform for miRNA detection in confined 3D nanospace with high sequence-specificity and sensitivity. After PMO was covalently immobilized on the nanochannel surface, hybridization between PMO-miRNA took place, making the miRNA detection highly sensitive and specific. Moreover, the nanochannel also showed high response and robust anti-interference when challenged in serum samples. The unique 3D geometry of the nanochannels enlarged surface area for the functionalization of probe molecule and thus improved the affinity between probe and target molecule. The PMO functionalized nanochannel could specifically discriminate Let-7b from miR-21, and Let-7c. In addition, this nanochannel biosensor achieved sensitivity as high as 1 fM in PBS and 10 fM in serum sample, respectively. It is anticipated that such a new method will benefit miRNA detection in clinical diagnosis with high sensitivity and specificity.

## ASSOCIATED CONTENT

The Supporting Information is available free of charge on the ACS Publications website at DOI…

FESEM images of nanochannels, the stability of functionalized nanaochannels, optimization of the experimental condition and detection limit of various methods for DNA sensing based on DNA-miRNA hybridization

## AUTHOR INFORMATION

### Corresponding Author

*G.-J. Zhang. Tel: +86-27-68890259. Fax: +86-27-68890259.

E-mail: zhanggj@hbtcm.edu.cn.

**Notes:** The authors declare no competing financial interest.

## ACKNOWLEDGMENT

We gratefully acknowledge financial support from the National Natural Science Foundation of China (NOs. 21405034, 21475037 and 21675041).

## REFERENCES

(1) Nilsen, T. W. *Trends Genet.* **2007**, *23*, 243-249.

(2) Stefani, G.; Slack, F. J. *Nat. Rev. Mol. Cell Biol.* **2008**, *9*, 219-230.

(3) Li, Y.; Kowdley, K. V. Genomics. *Proteomics Bioinf.* **2012**, *10*, 246-253.

(4) Guay, C.; Regazzi, R. *Nat. Rev. Endocrinol.* **2013**, *9*, 513-521.

(5) Kloosterman, W. P.; Plasterk, R. H. *Dev. Cell.* **2006**, *11*, 441-450.

(6) Shi, X. B. *Cell Cycle*. **2008**, *7*, 1529-1538.

(7) Esquela-Kerscher, A.; Slack, F. J. *Nat. Rev. Cancer*. **2006**, *6*, 259-269.

(8) Johnson, S. M. *Cell* **2005**, *120*, 635-647.

(9) Calin, G. A.; Sevignani, C.; Dumitru, C. D. *Proc. Natl. Acad. Sci. USA*. **2004**, *101*, 2999-3004.

(10)Lagos-Quintana, M.; Rauhut, R.; Lendeckel, W.; Tuschl, T. *Science* **2001**, *294*, 853-858.

(11) Ramkissoon, S. H.; Mainwaring, L. A.; Sloand, E. M.; Young, N. S.; Kajigaya, S. *Mol. Cell. Probes* **2006**, *20*, 1-4.

(12) Takada, S.; Berezikov, E.; Yamashita, Y.; Lagos-Quintana, M.; Kloosterman, W. P.; Enomoto, M.; Hatanaka, H.; Fujiwara, S.; Watanabe, H.; Soda, M.; Choi, Y. L., Plasterk, R. H.; Cuppen, E.; Mano, H. *Nucleic Acids Res*. **2006**, *34*, e115.

(13) Pritchard, C. C.; Cheng, H. H.; Tewari, M. *Nat. Rev. Genet*. **2012**, *13*, 358-369.

(14) Smith, S. M.; Murray, D. W. *Methods Mol. Biol.***2012**, *823*, 119-138.

(15) Raymond, C. K.; Roberts, B. S.; Garrett-Engele, P.; Lim, L. P.; Johnson, J. M. *RNA* **2005**, *11*, 1737-1744.

(16) Li, J.; Yao, B.; Huang, H.; Wang, Z.; Sun, C.; Fan, Y.; Chang, Q.; Li, S.; Wang, X.; Xi, J. Z. *Anal. Chem*. **2009**, *81*, 5446-5451.

(17) Cai, B. J.; Huang, L.; Zhang, H.; Sun, Z. Y.; Zhang, Z. Y.; Zhang, G. J. *Biosens. Bioelectron*. **2015**, *74*, 329-334,

(18) Sun, Z. Y.; Han, C. P.; Song, M. M.; Wen, L.; Tian, D. M.; Li, H. B.; Jiang, L. *Adv. Mater.* **2014**, *26*, 455-460.

(19) Sun, Z. Y.; Han, C. P.; Wen, L.; Tian, D. M.; Li, H. B.; Jiang, L. *Chem. Commun.* **2012**, *48*, 3282-3284.

(20) Sun, Z. Y.; Zhang, F.; Zhang, X. Y.; Tian, D. M.; Li, H. B.; Jiang, L. *Chem. Commun.***2015**, *51*, 4823-4826.

(21) Liu, N. N.; Yang, Z. K.; Lou, X. D.; Wei, B. M.; Zhang, J. T.; Gao, P. C.; Hou, R. Z.; Xia, F. *Anal. Chem.* **2015**, *87*, 4037-4041.

(22) Guo, W.; Hong, F.; Liu N. N.; Huang, J. Y.; Wang, B.; Duan, R. X.; Lou, X. D.; Xia, F. *Adv. Mater***. 2015**, *12*, 2090-2095.

(23) Wen, L.; Sun, Z. Y.; Han, C. P.; Imene, B.; Tian, D. M.; Jiang, L.; Li, H. B. *Chem. Eur. J.* **2013**, *19*, 7686-7690.

(24) Xu, Y. L.; Sui, X.; Guan, S.; Zhai, J.; Gao, L. C. *Adv. Mater.* **2015**, *27*, 1851-1855.

(25) Vlassiouk, I.; Kozel, T. R.; Siwy, Z. S. *J Am Chem Soc* **2009**, *131*, 8211-8220.

(26) Ali, M.; Nasir, S.; Ensinger, W. *Chem. Commun*. **2015**, *51*, 3454-3457.

(27) Liu, N. N. ; Jiang, Y. N. ; Zhou, Y. H. ; Xia, F. ; Guo, W. ; Jiang, L. *Angew. Chem. Int. Ed*. **2013**, *52*, 2007-2011.

(28) Ali, M.; Neumann, R.; Ensinger, W. *ACS Nano* **2010**, *4*, 7267-7274.

(29) Farimani, A. B.; Min, K.; Aluru, N. R. *ACS Nano* **2014**, *8*, 7914-7922.

(30) Sun, Z. Y.; Liao, T. B.; Zhang, Y. L.; Shu, J.; Zhang, H.; Zhang, G. J. *Biosens. Bioelectron*. **2016**, *86*, 194-201.

(31) Ali, M.; Yameen, B.; Cervera, J.; Ramirez, P.; Neumann, R.; Ensinger, W.; Knoll, W.; Azzaroni, O. *J. Am. Chem. Soc*. **2010**, *132*, 8338-8348.

(32) Daiguji, H.; Yang, P. D.; Majumdar, A. *Nano Lett.* **2004**, *4*, 137-142.

(33) Ramirez, P.; Mafe, S.; Aguilella, V. M.; Alcaraz, A. *Phys. Rev. E.* **2003**, *68*, 011910.

(34) Summerton, J. Discoveries in Antisense Nucleic Acids; Brakel, C., Eds.; Portfolio Publishing Co., Woodlands, TX. 1989.

(35) Summerton, J.; Weller, D. *Antisense Nucleic Acid Drug Dev*. **1997**, *7*, 187-195.

(36) Zhang, G. J.; Luo, Z. H. H.; Huang, M. J.; Tay, G. K. I.; Lim, E. J. A. *Biosens. Bioelectron.***2010**, *25*, 2447-2453.

(37) Li, S. J.; Li, J.; Wang, K.; Wang, C.; Xu, J. J.; Chen, H. Y.; Xia, X. H.; Huo, Q. A *ACS Nano*. **2010**, *4*, 6417-6424.

(38) Zu, Y. B.; Ting, A. L.; Yi, G. S.; Gao, Z. Q. *Anal. Chem.* **2011**, *83*, 4090-4094.

(39) Li, S. J.; Li, J.; Wang, K.; Wang, C.; Xu, J. J.; Chen, H. Y.; Xia, X. H.; Huo, Q. *ACS Nano*. **2010**, *4*, 6417-6424.

(40) Wang, X.; Smirnov, S. *ACS Nano*. **2009**, *3*, 1004-1010.

(41) Gao, H. Li.; Wang, M.; Wu, Z. Q.; Wang, C.; Wang, K.; Xia, X. H. *Anal. Chem*. **2015**, 87, 3936-3941.

(42) Hermanson, G. T. *Bioconjugate Techniques*; Academic Press: San Diego, CA, 1996.

(43) Cai, B. J.; Huang, L.; Zhang, H.; Sun, Z. Y.; Zhang, Z. Y.; Zhang, G. J. *Biosens. Bioelectron*. **2015**, *74*, 329-334.

(44) Wang, W.; Kong, T.; Zhang, D.; Zhang, J. N.; Cheng, G. S. *Anal. Chem.* **2015**, *87*, 10822-10829.

(45) Koo, K. M.; Carrascosa, L. G.; Shiddiky, M. J. A.; Trau, M. *Anal. Chem.* **2016**, *88*, 2000-2005.

(46) Liao, R.; He, K.; Chen, C.; Chen, X.; Cai, C. *Anal. Chem.* **2016**, *88*, 4254-4258.

(47) Miao, J.; Wang, J.; Guo, J.; Gao, H.; Han, K.; Jiang, C.; Miao, P.; *Sci. Rep.* **2016**, 6: 32219 | DOI: 10.1038/srep32219.

(48) Qiu, X.; Liu, X.; Zhang, W.; Zhang, H.; Jiang, T.; Fan, D.; Luo, Y. *Anal. Chem.* **2015**, *87*, 6303-6310.

**Figure captions:**

**Figure 1.** Schematic illustration of the PMO-functionalized nanochannel biosensor for miRNA detection.

**Figure 2.** A) Current-voltage (I-V) characteristics of conical nanochannel with tip d = 51nm and base D = 1.1 μm, bare nanochannel(■), immobilized PMO probe (●), and BSA blocking (◆) on the channel surface, respectively. I-V curves were measured in 0.5×PBS (pH = 7.1) solution. B) Wide survey of XPS analysis on the bare and the PMO-modified PET surface, respectively. C) Narrow survey of XPS analysis on P element on the bare and the PMO-modified PET surface, respectively.

**Figure 3.** A) Schematic illustration showing the specificity of the nanochannel biosensor for miRNA detection. B) I-V curves of the PMO functionalized nanochannel biosensor after treated with 1 nM miR-21, let-7c, and let-7b, respectively. In this experiment, 0.5×PBS, pH 7.1 acted as the control (black line). C) The relative ion current change ratios of the modified nanochannel in the presence of 1 nM concentration of the above-mentioned 3 miRNA strands.

**Figure 4.** A) LSCM observation of the nanochannels before and after two different Cy3 fluorophore labeled miRNA (Cy3-miRNA-21 and Cy3-let-7b, respectively) hybridized with PMO on the channel surface. B) Wide survey of XPS analysis on the PMO-modified and Cy3-let7b hybridized PET surface, respectively. Narrow survey of XPS analysis on P element (C) and S element (D) on the PMO-modified and Cy3-let7b hybridized PET surface, respectively.

**Figure 5.** A) I-V curves of the nanochannel biosensor hybridized with let-7b at a

series of concentrations (100 aM-1 nM), and B) The relative ion current change versus various concentrations.

**Figure 6.** A) The relative ion current change ratios at -2 V ($I-I_0/I_0$) of 4 modified nanochannels in the presence of 1 nM concentration of Let-7b; B) Reusability of the PMO modified nanochannels biosensors. PMO/miRNA hybridization and denaturation were run 4 times on the same nanochannel at -2 V (hybridization: red squares and denaturation: blue squares).

**Figure 7.** A) I-V curves of the nanochannel biosensor hybridized with let-7b at a series of concentrations (100 aM-1 nM) in 5 % fetal bovine serum sample and B) The relative ion current change versus various concentrations.

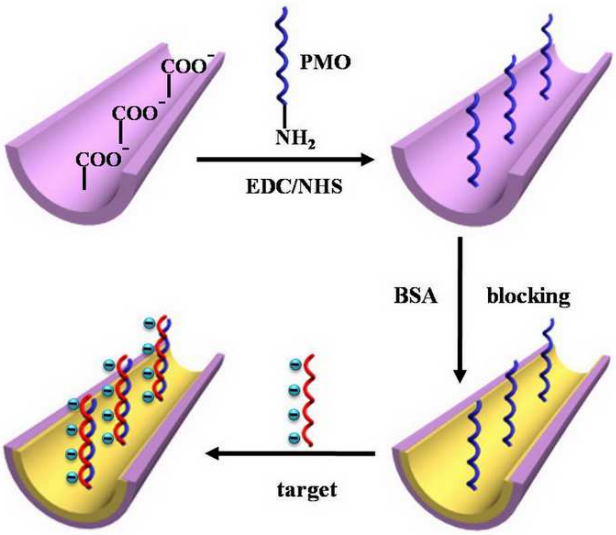


**Figure 1**

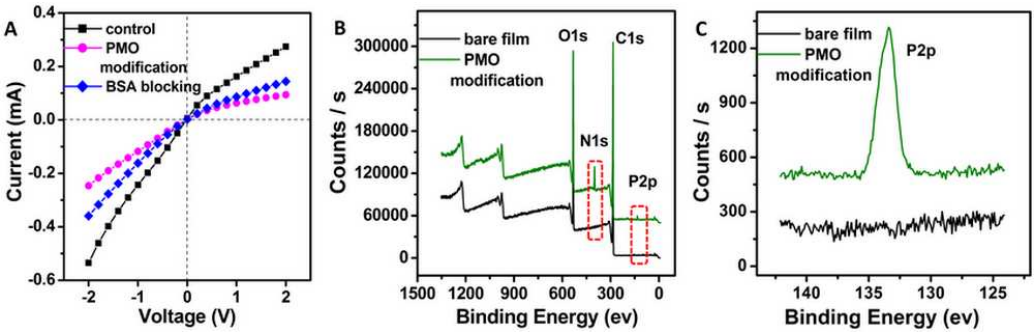
A
control
PMO modification
BSA blocking
Current (mA)
Voltage (V)
B
bare film
PMO modification
O1s
C1s
N1s
P2p
Counts / s
Binding Energy (ev)
C
bare film
PMO modification
P2p
Counts / s
Binding Energy (ev)

**Figure 2**

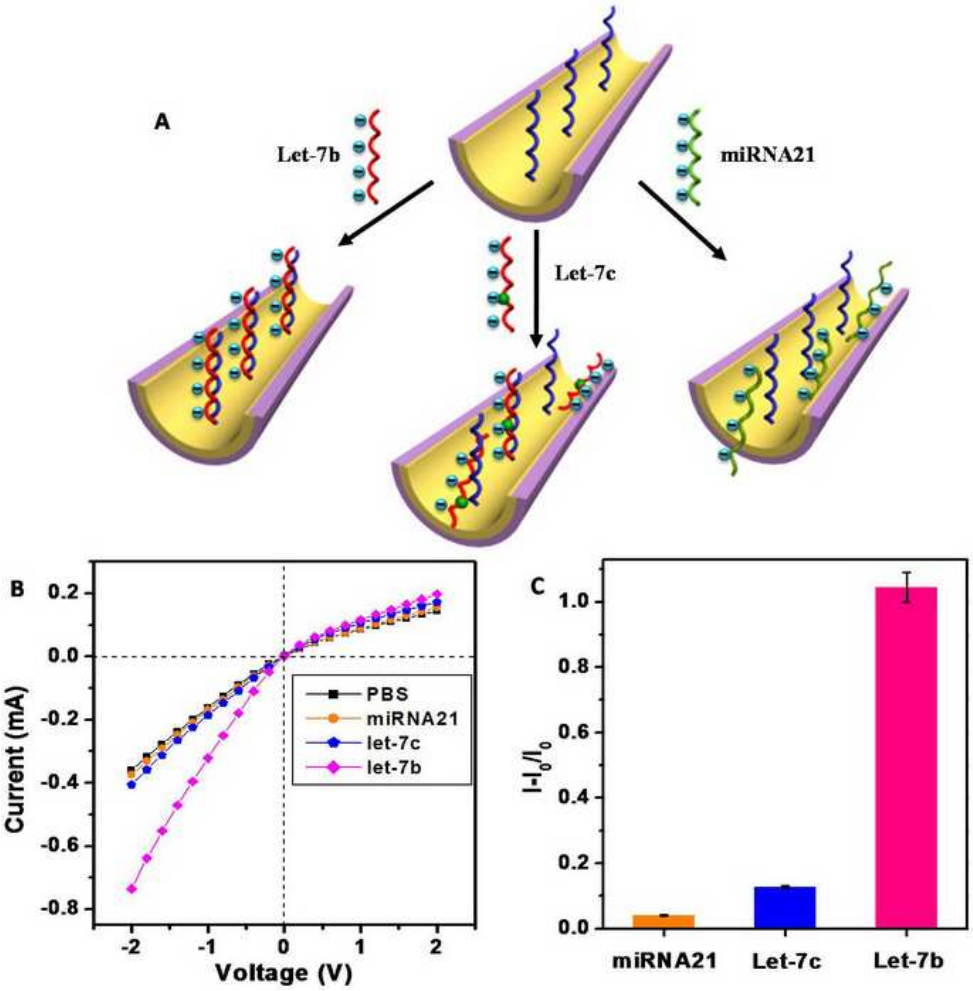
A
Let-7b
miRNA21
Let-7c
B
Current (mA)
Voltage (V)
PBS
miRNA21
let-7c
let-7b
C
I-I0/I0
miRNA21
Let-7c
Let-7b

**Figure 3**

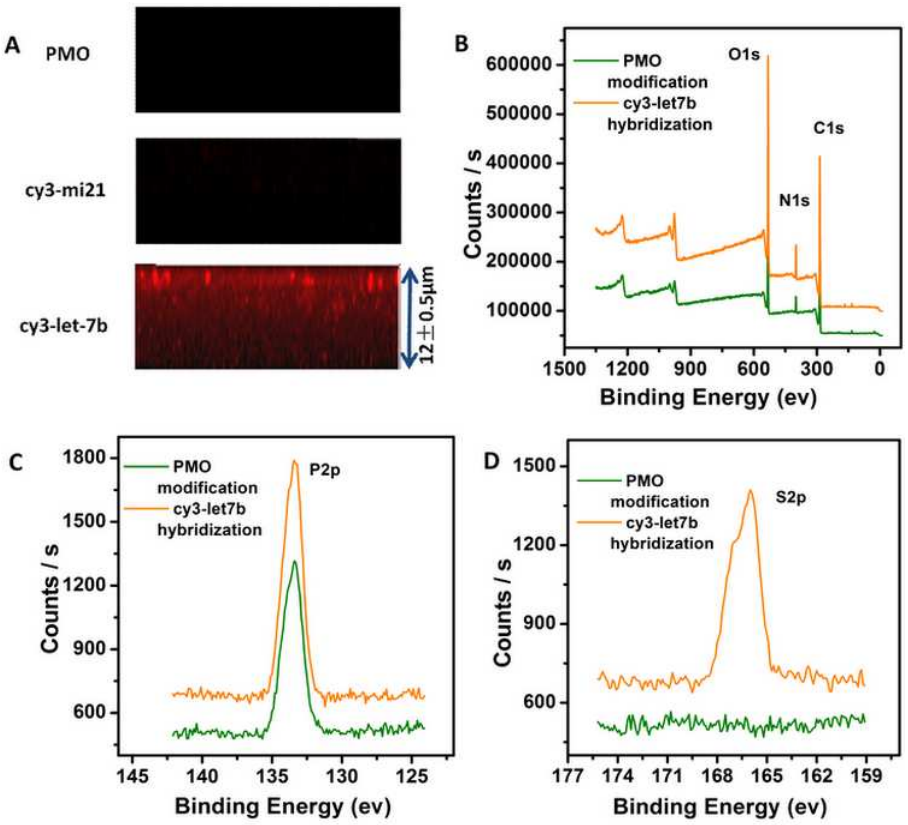
A
PMO
cy3-mi21
cy3-let-7b
12±0.5μm
B
PMO modification
cy3-let7b hybridization
O1s
C1s
N1s
Counts / s
Binding Energy (ev)
C
PMO modification
cy3-let7b hybridization
P2p
Counts / s
Binding Energy (ev)
D
PMO modification
cy3-let7b hybridization
S2p
Counts / s
Binding Energy (ev)

**Figure 4**

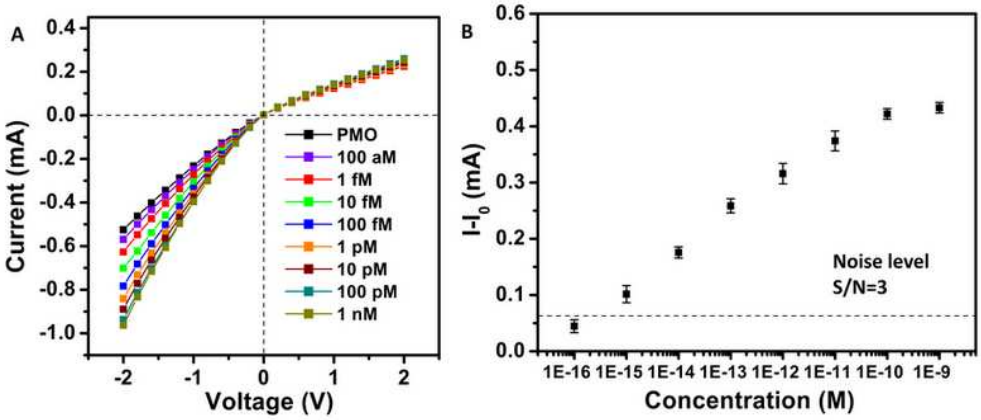
A
Current (mA)
Voltage (V)
PMO
100 aM
1 fM
10 fM
100 fM
1 pM
10 pM
100 pM
1 nM
B
I-I0 (mA)
Concentration (M)
Noise level
S/N=3
1E-16 1E-15 1E-14 1E-13 1E-12 1E-11 1E-10 1E-9

**Figure 5**

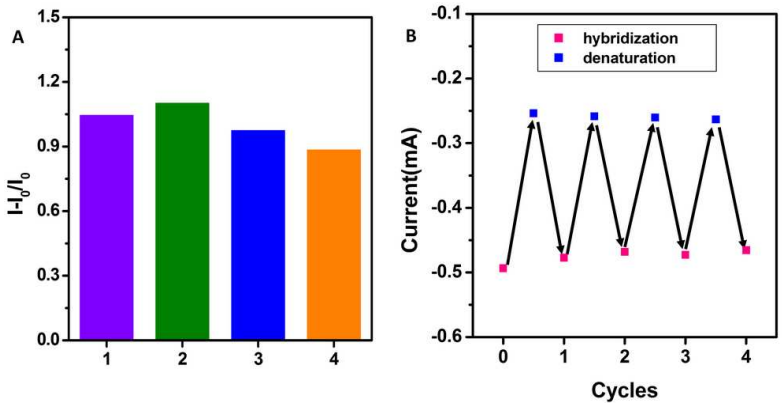
A
1.5
1.2
0.9
0.6
0.3
0.0
I-I0/I0
1
2
3
4
B
-0.1
-0.2
-0.3
-0.4
-0.5
-0.6
Current(mA)
hybridization
denaturation
0
1
2
3
4
Cycles

**Figure 6**

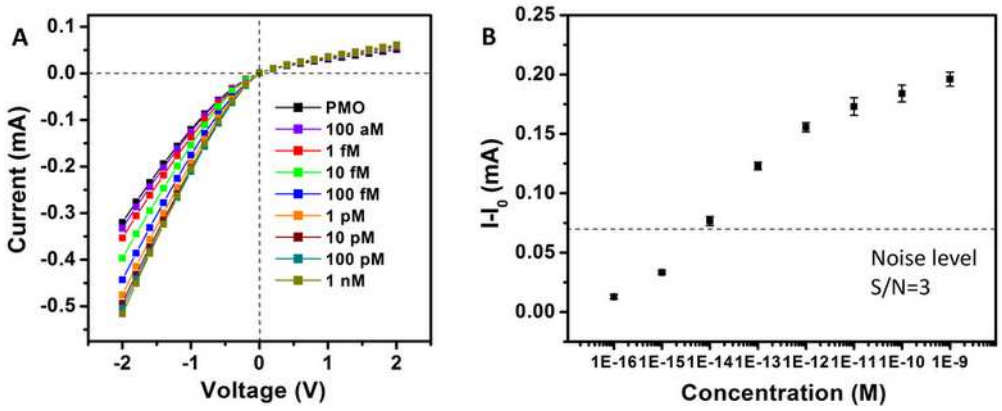
A
Current (mA)
Voltage (V)
PMO
100 aM
1 fM
10 fM
100 fM
1 pM
10 pM
100 pM
1 nM
B
I-I0 (mA)
Concentration (M)
Noise level
S/N=3

**Figure 7.**

**TOC**